A More Accurate Analysis and Design of Coaxial-to-Rectangular Waveguide End Launcher

SAAD MICHAEL SAAD, SENIOR MEMBER, IEEE

Abstract — A new, more accurate electromagnetic model is developed for the analysis of the coaxial-to-rectangular waveguide transition of the end-launcher type. As an alternative to the well-known modeling via a coupling loop, the new model describes the coupling mechanism in terms of an excitation probe which is fed by a transmission line intermediate section. The two models have a few analytical steps in common, but expressions of the probe model are easier to derive and compute. The two models are presented together with numerical examples and experimental verification. The superiority of the probe model is illustrated, and a design method yielding a maximum *VSWR* of 1.035 over 13 percent bandwidth is outlined.

I. Introduction

In many applications, the end-launcher transition (Fig. 1) is a preferred choice over other types of coaxial-to-waveguide transitions. Examples are encountered where the collinearity of the coaxial line and the waveguide is imposed by antenna feeder design requirements, or where a large number of such transitions are to be optimally arranged in a limited space, as in phased array antenna systems.

This type of transition, which converts the coaxial TEM mode into a waveguide dominant mode, has been analyzed before. Utilizing an electromagnetic model of loop coupling, Deshpande *et al.* obtained an expression for the input impedance of the rectangular [1] and circular [2] waveguide cases. However, such a loop coupling model, as will be verified, has limited accuracy and is valid only for loops of small size.

In this paper, we present a more accurate electromagnetic model of the subject transition. Instead of loop coupling, the new model considers the region $0 \leqslant z \leqslant L_1$ as merely a transmission line intermediate section feeding a probe BC, which excites the waveguide. The analyses of these loop and probe coupling models are presented in Sections II–IV for the rectangular waveguide case. In Section V, the range of validity of each model is illustrated numerically and verified experimentally. In Section VI, design methods and applications are demonstrated, and Section VII is a conclusion.

Manuscript received September 26, 1988; revised September 6, 1989.
The author is with the Andrew Corporation, 10500 W. 153rd Street, Orland Park, IL 60462.
IEEE Log Number 8931996.

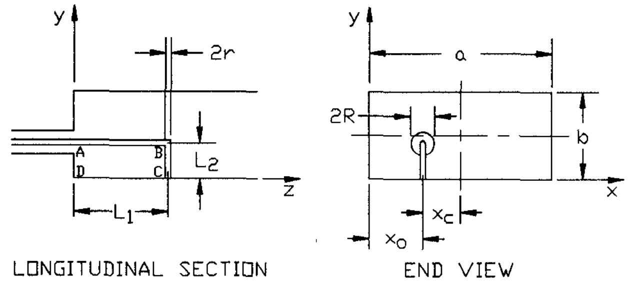

Fig. 1. End-launcher coaxial-to-rectangular waveguide transition.

II. The Loop Coupling Model

The loop coupling approach, explained in [1], is outlined here because it has a few steps in common with the new probe coupling model. Details of the analysis, however, will not be repeated except when needed to construct the probe coupling model, or when a major difference from [1] occurs, e.g., our use of the Coulomb, rather than Lorentz, vector potential.

Starting with the stationary formula [3] for the input impedance at $z=0$ in Fig. 1,

$$Z_{\text{in}} = -\frac{1}{I_{\text{in}}^2}\int_V \boldsymbol{E}_{ABC}\cdot \boldsymbol{J}_{ABC}\, dV \tag{1}$$

a closed-form solution for Z_{in} is obtained through the following three steps. First, arm ABC is assumed to support a sinusoidal trial current density:

$$\boldsymbol{J}_{AB}(z) = \boldsymbol{a}_z \frac{I_0}{2\pi r}\cos k(L_1+L_2-|z|) \qquad \text{along } AB \tag{2a}$$

$$\boldsymbol{J}_{BC}(y) = -\boldsymbol{a}_y \frac{I_0}{2\pi r}\cos ky \qquad \text{along } BC \tag{2b}$$

where k is the free-space wavenumber and I_{in} is the input current at point A:

$$I_{\text{in}} = I_0 \cos k(L_1+L_2). \tag{3}$$

Second, the electric field $\boldsymbol{E}_{ABC}$ is derived from the vector potential through the special relation representing the Coulomb gauge:

$$\boldsymbol{E}_{ABC} = -j\omega \boldsymbol{A}_{ABC}. \tag{4}$$

This relation allows us to directly integrate Smythe's expression [4] of the three-dimensional vector potential

0018-9480/90/0200-0129$01.00 ©1990 IEEE

caused by a z-directed current element at (x', y', z'), its image in the $z=0$ waveguide wall, and their infinite set of images in all other walls, i.e.,

$$\begin{aligned}\boldsymbol{A}^z = \int_{-L_1}^{L_1} I(z')\,dz' \sum_{m=1}^{\infty}\sum_{n=1}^{\infty} \frac{j2\mu}{k^2 ab\beta_{mn}} \sin(a'x')\sin(b'y') \\ \cdot\Big\{ j\pi\beta_{mn}\Big[\boldsymbol{a}_x \frac{m}{a}\cos(a'x)\sin(b'y) \\ + \boldsymbol{a}_y \frac{n}{b}\sin(a'x)\cos(b'y)\Big] \\ - \boldsymbol{a}_z k_{cmn}^2 \sin(a'x)\sin(b'y)\Big\} e^{-j\beta_{mn}|z-z'|}. \end{aligned} \quad (5a)$$

Similarly, for a y-directed current element,

$$\begin{aligned}\boldsymbol{A}^y = \int_0^{L_2} I(y')\,dy' \sum_{m=1}^{\infty}\sum_{n=0}^{\infty} \frac{j2\mu}{(1+\delta_{0n})k^2 ab\beta_{mn}} \\ \cdot \sin(a'x')\cos(b'y') \\ \cdot\big[\boldsymbol{a}_x a'b'\cos(a'x)\sin(b'y) \\ - \boldsymbol{a}_y (k^2 - b'^2)\sin(a'x)\cos(b'y) \\ - \boldsymbol{a}_z j\beta_{mn} b' \sin(a'x)\sin(b'y)\big] e^{-j\beta_{mn}|z-z'|} \end{aligned} \quad (5b)$$

$$a' = m\pi/a \qquad b' = n\pi/b \quad (5c)$$

where k_{cmn} is the cutoff wavenumber and δ_{0n} is the Kronecker delta. By substituting from (2) in (5), performing the line integrations in (5), and then substituting in (4), an expression for the electric field is obtained. Because a given current element may excite only the modes that have an electric field along it, we note that TE modes are excited only by section BC of the loop, while TM modes are excited by both sections AB and BC.

Third, we substitute from (2)–(4) into (1) and perform the involved integrations to obtain (6)–(28) which, together with the equivalent circuit of Fig. 2, describe Z_{in}. The justification of this circuit is explained in [2] and [3], but the following is particular to this analysis. The reactive component jX_2, associated with higher order modes, is derived by considering the interaction between the current in section AB and the electric field excited by the full length of arm ABC, not just section AB as in [1] and [2]. Likewise, the interaction between the current in section BC and the electric field excited by arm ABC results in the resistive component R_{in} and the reactive component jX_3, both associated with the dominant mode, in addition to the reactive component jX_1 associated with higher order modes. The derivation concludes in

$$Z_{in} = R_{in} + j(X_1 + X_2 + X_3) \quad (6)$$

$$R_{in} = p^2 S_1^2 Z_g \quad (7)$$

$$X_3 = p^2 S_1 C_1 Z_g \quad (8)$$

$$X_1 = \frac{120\pi}{kab}\left(\frac{I_0}{I_{in}}\right)^2 \sum_{m=1}^{\infty} S_6 S_{6r} \sum_{n=0}^{\infty} (X_{1nAB} + X_{1nBC}) \qquad (m,n) \neq (1,0) \quad (9)$$

$$X_{1nAB} = 2k_{cmn}^{-2} b' L_2 S_7 S_9 f_1 e^{-\alpha_{mn}(L_1 + r)} \quad (10a)$$

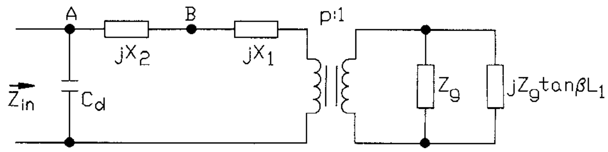

Fig. 2. Equivalent circuit of transition of Fig. 1.

$$X_{1nBC} = \frac{1+\delta_{0n}}{4\alpha_{mn}} S_9^2 (k^2 - b'^2) L_2^2 (1 - e^{-2\alpha_{mn}L_1}) e^{-\alpha_{mn} r} \quad (10b)$$

$$X_2 = \frac{120\pi}{kab}\left(\frac{I_0}{I_{in}}\right)^2 \sum_{m=1}^{\infty} S_6 S_{6r} X_{2m} \quad (11)$$

$$X_{2m} = -\frac{2b}{\pi} C_2^2 [K_0(a'r) - K_0(2a'L_2)] + \sum_{n=1}^{\infty} (X_{2nAB} + X_{2nBC} + X_{2ns}) \quad (12)$$

$$X_{2nAB} = 2 S_7 S_{7r} f_2 \alpha_{mn} / k_{cmn}^2 \quad (13)$$

$$X_{2nBC} = b' L_2 S_{7r} S_9 f_3 \alpha_{mn} / k_{cmn}^2 \quad (14)$$

$$X_{2ns} = -\frac{2b}{\pi} C_2^2 \{ K_0[a'(2nb + r)] + K_0[a'(2nb - r)] - K_0[2a'(nb + L_2)] - K_0[2a'(nb - L_2)] \} \quad (15)$$

$$Z_g = \omega\mu/\beta \quad (16)$$

$$p^2 = \frac{2}{k^2 ab}\left(\frac{I_0}{I_{in}}\right)^2 S_4 S_{4r} S_2^2 \quad (17)$$

$$f_1 = kS_3 - kS_2 \cosh\alpha_{mn}L_1 + \alpha_{mn} C_2 \sinh\alpha_{mn}L_1 \quad (18)$$

$$f_2 = \frac{2k}{\alpha_{mn}} S_3 \left(C_3 + \frac{kS_3}{\alpha_{mn}}\right) + \left(\frac{kS_2}{\alpha_{mn}}\right)^2 + f_4\left(f_4 - \frac{4kS_3}{\alpha_{mn}}\right) + C_2^2\left(\frac{k_{cmn}}{\alpha_{mn}} - 1\right) \quad (19)$$

$$f_3 = e^{-\alpha_{mn}L_1}(2C_3 - f_4) + \frac{k}{\alpha_{mn}} S_2 + C_2\left(\frac{2}{b'L_2} C_2 \frac{S_7}{S_9}\frac{k_{cmn}}{\alpha_{mn}} - 1\right) \quad (20)$$

$$f_4 = e^{-\alpha_{mn}L_1}\left(C_2 + \frac{kS_2}{\alpha_{mn}}\right) \quad (21)$$

$$S_1 = \sin\beta L_1, \qquad C_1 = \cos\beta L_1 \quad (22)$$

$$S_2 = \sin kL_2, \qquad C_2 = \cos kL_2 \quad (23)$$

$$S_3 = \sin k(L_1 + L_2), \qquad C_3 = \cos k(L_1 + L_2) \quad (24)$$

$$S_4 = \sin\frac{\pi x_0}{a} \qquad S_{4r} = \sin\frac{\pi}{a}(x_0 - r) \quad (25)$$

$$S_6 = \sin a'x_0 \qquad S_{6r} = \sin a'(x_0 - r) \quad (26)$$

$$S_7 = \sin b'L_2 \qquad S_{7r} = \sin b'(L_2 + r) \quad (27)$$

$$S_9 = \frac{\sin(b'-k)L_2}{(b'-k)L_2} + \frac{\sin(b'+k)L_2}{(b'+k)L_2}. \quad (28)$$

It is worth mentioning that the series in (12) is a transformation of what was originally a series with prohibitively slow convergence. The transformation is analogous to that of [5, eq. (5.63)].

III. The Probe Coupling Model

In contrast to the loop coupling approach, the probe coupling one makes explicit the role of the TEM mode in the transition region $0 \leqslant z \leqslant L_1$ (Fig. 1). This is done by considering section BC as a probe which, while exciting the rectangular waveguide, is itself fed by a coaxial intermediate section having AB as its inner conductor. By intuition, the significance of the TEM mode should increase as L_1 increases. Because it ignores the TEM mode, the loop coupling model is valid only for small loops. In the probe coupling model, therefore, the coupling between the coaxial line and the waveguide is accomplished in two stages. The first stage affects only the coaxial outer conductor, which, upon transformation into a rectangular shape at $z=0$, presents to the coaxial line a shunt capacitance C_d (Fig. 2), while still supporting the TEM mode in the rectangular coaxial line section $0 \leqslant z \leqslant L_1$. The second stage is the coupling between the rectangular coaxial line and the rectangular waveguide. This is achieved by probe BC, which excites the rectangular TE_{10} mode together with higher order modes.

According to the above description, the probe coupling model may be implemented through the following steps. The first step is to derive the input impedance at plane BC. From (1),

$$Z_{BC} = -\frac{1}{I_{\text{in}}^2}\int_V \boldsymbol{E}_{ABC}\cdot \boldsymbol{J}_{BC}\, dV \tag{29}$$

with $\boldsymbol{J}_{BC}$ given by (2b), and I_{in} is now

$$I_{\text{in}} = I_0 \cos kL_2. \tag{30}$$

By deriving $\boldsymbol{E}_{ABC}$ as shown above for the loop coupling model, (29) results in

$$Z_{BC} = R_{BC} + j(X_1 + X_3) \tag{31}$$

where R_{BC}, X_1, and X_3 are given by relevant equations in the set (7)–(28), but substituting I_{in} with (30).

In the second step, the impedance Z_{BC} is transformed along the rectangular coaxial line from plane BC to plane AD using the formula

$$Z_{\text{in}} = R_{\text{in}} + jX_{\text{in}} = Z_0 \frac{Z_{BC} + jZ_0 \tan kL_1}{Z_0 + jZ_{BC}\tan kL_1}. \tag{32}$$

With simple manipulation,

$$R_{\text{in}} = R_{BC}/D \tag{33}$$

$$X_{\text{in}} = \frac{1}{D}\left[(X_1 + X_3)\cos 2kL_1 + \frac{Z_0}{2}(1-G)\sin 2kL_1\right] \tag{34}$$

$$D = \cos^2 kL_1 - \frac{X_1 + X_3}{Z_0}\sin 2kL_1 + G\sin^2 kL_1 \tag{35a}$$

$$G = \frac{R_{BC}^2 + (X_1 + X_3)^2}{Z_0^2} \tag{35b}$$

where Z_0 is the characteristic impedance of a round wire displaced from the center of a rectangular outer conductor. To the author's knowledge, such an impedance has not been derived before, but an approximate expression may be borrowed from the trough line case [6], i.e.,

$$Z_0 = 138\left[\log\left(\frac{2b}{\pi}\tanh\frac{\pi x_0}{b}\right) - Z_1\right] \tag{36}$$

$$Z_1 = \sum_{m=1}^{\infty} \log\frac{1+U_m^2}{1-V_m^2} \tag{37}$$

$$U_m = \sinh\frac{\pi x_0}{b}\Big/\cosh\frac{m\pi a}{b} \tag{38}$$

$$V_m = \sinh\frac{\pi x_0}{b}\Big/\sinh\frac{m\pi a}{x_0}. \tag{39}$$

Expression (36) yields accurate results in the limiting cases available in the literature, e.g., the round wire in a square outer conductor [7, p. 98]. Obviously, (36) may be replaced by a more accurate expression, if available, or by a numerically obtained value for Z_0, without affecting the integrity of this probe coupling model.

A comparison between (1)–(28) and (29)–(39) proves that the probe model expressions are simpler to derive and compute than those of the loop model. By eliminating the need to model the region $0 \leqslant z \leqslant L_1$ in terms of a reactance jX_2, the probe model saves a substantial part of the derivation and computer time. As for accuracy, the probe model avoids the truncation error of the series in (11) and (12). Also, by excluding the sinusoidal trial current distribution (2a) along AB from the derivation of Z_{in}, the probe model has fewer approximations.

IV. The Coaxial Step Discontinuity

As explained previously, the coaxial step discontinuity at $z=0$ (Fig. 1) may be represented by a capacitance C_d shunted to Z_{in} (Fig. 2). One approximate method of calculating C_d is by equating it to the capacitance due to a step in the outer conductor of a coaxial line, and taking the hypothetical radius r_o of the larger outer conductor such that its characteristic impedance Z_0, given by

$$Z_0 = 138 \log\frac{r_o}{r} \tag{40}$$

is equal to Z_0 given by (36) for the actual rectangular coaxial line section. Curves useful in obtaining C_d are given in [7, p. 111].

V. Numerical Examples and Experimental Verification

Two computer programs were developed to perform the numerical analyses associated with the above loop and probe coupling models. Each program computes the input impedance at the coaxial-to-waveguide junction for given design parameters a, b, r, R, L_1, L_2, and x_0 and frequency.

The transition models experimentally tested were basically two, but with adjustable dimensions to allow for measurement of different combinations of design parame-

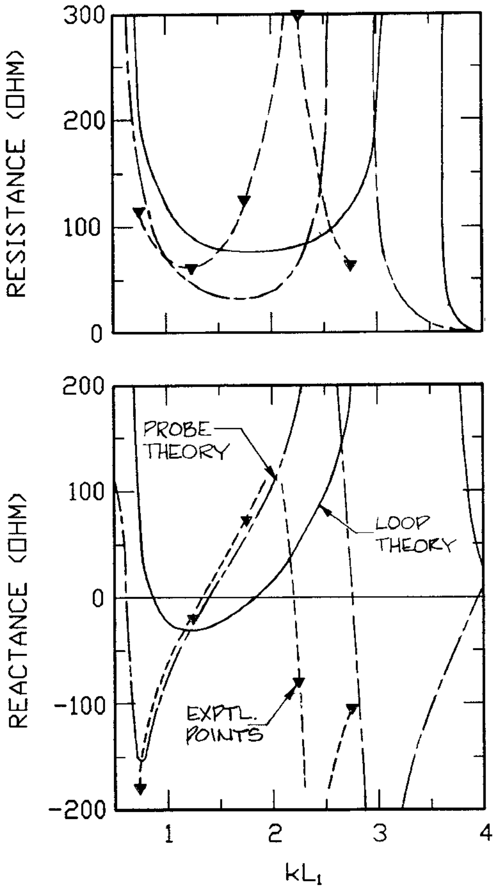

Fig. 3. Input impedance of a coaxial-to-WR229 transition. Comparison between two theoretical models and experiment. $L_2/b = 0.5, 2r = 0.174$ in., $x_c = 0$, frequency = 3.95 GHz.

ters. Each of the two test models comprised a WR229 (2.29×1.145 in.^{2}) connected to a 50 Ω coaxial line via a conductor ABC with $L_2/b = 0.5$, $x_c = 0$ or 0.473 in. and L_1 variable (Fig. 1). The inner and outer diameters of the coaxial were 0.174 and 0.398 in. in one model, and 0.341 and 0.784 in. in the other. To enable L_1 to vary in increments, an array of holes was tapped in the waveguide wall $y = 0$, and the metal post BC was firmly joined to the sliding inner conductor AB and the waveguide wall at C, via screws secured internally.

Fig. 3 shows a comparison between the loop and probe theories and experimental results for a transition having $L_2/b = 0.5$, $2r = 0.174$ in., and $x_c = 0$. The step discontinuity (presented in Section IV) is not included in the computations of Fig. 3 in order to examine how the two theoretical models compare on their own and to allow a fair comparison between the probe model and the loop models of [1] and [2], which did not account for such a step discontinuity.

In Fig. 3 both theoretical approaches offer good qualitative predictions of the input impedance over a substantial range of kL_1. Compared to the loop theory, however, the probe theory is of greater quantitative agreement with experiment throughout the shown range of kL_1. Of particular importance is that the probe theory is in much closer agreement with experiment in the range $kL_1 = 0.9$ to 1.4, where impedance matching can be achieved because R_{in} is in the range 50–75 Ω, commonly chosen for coaxial lines, and X_{in} is close to naught. It is also noticeable that the accuracy of the loop theory deteriorates considerably as the loop size increases. For example the reactance vanishes experimentally at $kL_1 = 1.3$ and 2.2, by the probe theory at $kL_1 = 1.37$ and 2.7, and by the loop theory at $kL_1 = 1.85$ and 4.2.

In view of the above, one may consider the possibility that the excellent agreement between the loop theory and experiment reported in [1] is not general but rather is particular to that L_1 and frequency. This possibility is also supported by the observation that at $kL_1 = 2.6$ (Fig. 3) our loop theory curves intersect with the experimental curve of the resistance and the inversion of the reactance, thus resulting in a misleadingly accurate *VSWR*. This could be the case with the loop theory of [1] as well. (Note that $kL_1 = 2.6$ is close to the center of their range of excellent agreement.) This possible particularity of the results in [1] is revealed because the comparison given here between theory and experiment is performed for the input impedance over a few octaves, rather than for *VSWR* over a 32 percent bandwidth as in [1].

Experimental verification of the probe theory is once again illustrated in Fig. 4. This time it is an offset transition, $x_c/a = 0.191$, $L_2/b = 0.5$, and $2r = 0.341$ in.

Adding the contribution of the coaxial step discontinuity, via the procedure of Section IV, consistently improves the agreement between theory and experiment. This is also true for the loop theory (not shown). It is now clear that the probe theory can predict optimum L_1 (that which results in a prescribed Z_{in}) with a maximum error of 0.15 in. (i.e., 0.05 λ_0 or $0.88r$) while maintaining exact prediction of both L_2 and x_c. This is valid for both the resistance and the reactance, especially in the useful design range $R_{in} = 50$–75 Ω and $X_{in} = 0$.

The magnitude of such an agreement is indeed excellent, since the difference between theory and experiment is less than the radius of the probe. This may mean, among other explanations, that the effective length of AB is somewhere between L_1 and $L_1 + r$, a phenomenon always associated with loops and probes made of conductors with finite radii.

VI. Design Applications

Having obtained such an accurate probe theory for the end-launcher coaxial-to-rectangular waveguide transition, the complete accurate design of such a waveguide transition is now possible. Specifically, theoretical curves of input impedance, such as those in Fig. 5 can be utilized to generate exact optimum values for a, b, L_2, x_c, r, and R, and a value for L_1 which is within r from its exact optimum value. Adjusting L_1 empirically for improved performance over the required frequency band and using a tuning post parallel to BC are common practices in the industry, especially because such a step is usually required to compensate for manufacturing tolerances.

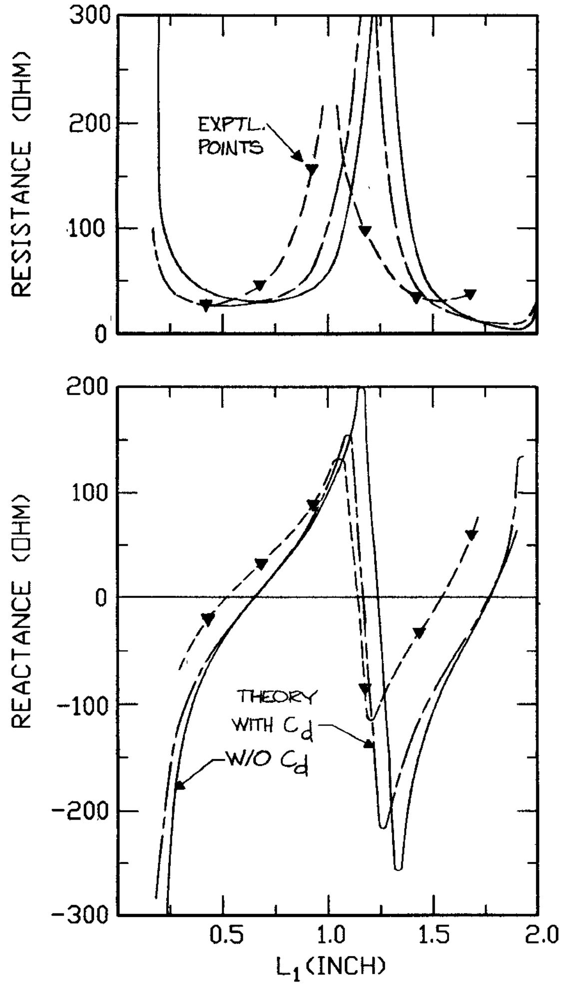

Fig. 4. Input impedance of a coaxial-to-WR229 transition. Comparison between probe theory and experiment showing effect of step discontinuity capacitance C_d. $L_2/b = 0.5$, $2r = 0.341$ in., $x_c/a = 0.191$, frequency = 3.95 GHz.

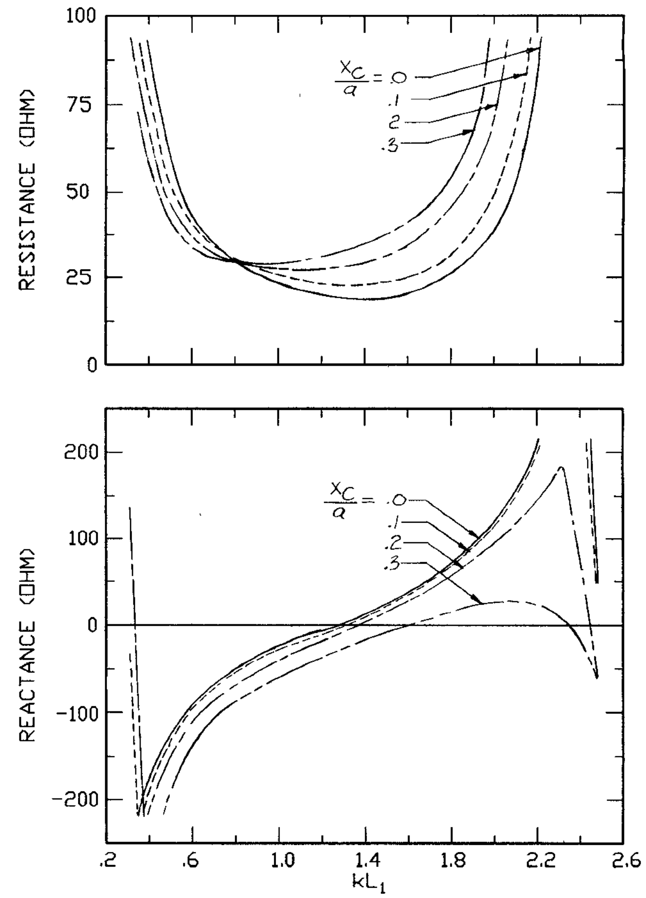

Fig. 5. Input impedance of a coaxial-to-WR229 transition: $L_2/b = 0.5$, $kr = 0.358$.

Depending on the application, a variety of design criteria and strategies may be employed, two of which are explained below.

A. Perfect Match at Midband

For narrow-band applications, a perfect match at midband may be selected as a design criterion. This requires simultaneous fulfillment at midband of two conditions:

$$R_{in} = Z_x \qquad X_{in} = 0 \tag{41}$$

where Z_x is the coaxial line characteristic impedance. From curves such as in Fig. 5, one can generate the curves of Fig. 6, which describe the locus of the combination (L_1, L_2, x_c) that simultaneously satisfies the two conditions of (41). An important finding is that the coaxial line has to be offset, in either the x or the y direction, in order to achieve perfect match at midband. This means that for impedance matching there must be a compromise in the mechanically desirable feature of a common axis for the coaxial and rectangular waveguides (e.g., to allow convenient rotation).

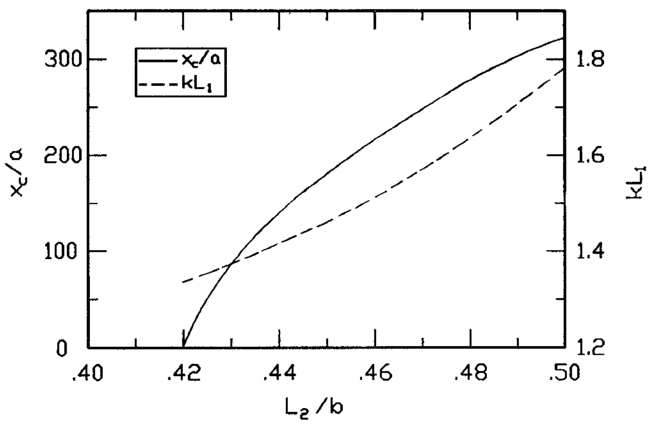

Fig. 6. Locus of kL_1, L_2/b, and x_c/a which results in a perfectly matched transition between a 50 Ω coaxial and WR229 at 3.95 GHz.

B. Minimum VSWR over a Band

For wide-band applications, a minimum *VSWR* over a frequency range is normally preferred over the above method of a perfect match at midband. The variation of input impedance with L_1 over the frequency band 3.7–4.2 GHz is given in Fig. 7 for a coaxial-to-WR229 transition with $L_2/b = 0.442$ and $x_c/a = 0.2$. It is obvious that while an almost constant R_{in} over the band is achievable (at $L_1 = 0.74$ in.), one can only aim at minimum variation in X_{in}. To achieve an optimum design, therefore, one

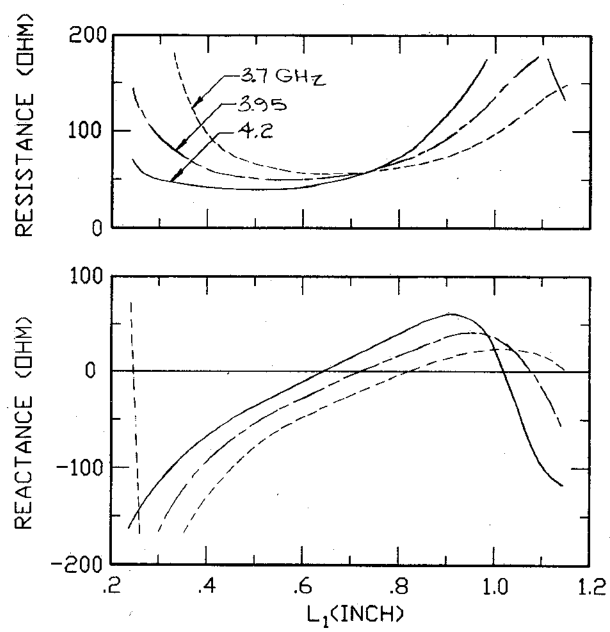

Fig. 7. Input impedance of a coaxial-to-WR229 transition over the 3.7–4.2 GHz band. $L_2/b = 0.442$, $x_c/a = 0.2$, and $2r = 0.341$ in.

should minimize the variation of *VSWR* over the operating frequency band using a standard optimization algorithm.

It is worth mentioning that by applying this design method (together with the probe theory and computer program), and adding one tuning post parallel to *BC*, it was possible to realize a transition with a *VSWR* better than 1.035 over the band 3.7–4.2 GHz [8].

VII. Conclusion

A new electromagnetic model for the analysis of the coaxial-to-rectangular waveguide end launcher has been constructed. By analytical presentation and experimental verification, the new model was found to be easier to derive, to take less time to compute, and to be more accurate than a previous model. This allows the design to be put on a reliable quantitative basis.

The characteristics of the end launcher were illustrated by numerical and experimental examples, two design procedures were presented, and a transition exhibiting −35 dB return loss over a 13 percent bandwidth was developed.

The new model applied in this paper to the coaxial-to-rectangular waveguide end launcher can readily be employed to analyze the coaxial-to-circular waveguide and the stripline-to-waveguide end launchers, thus providing more accurate and simpler solutions than those available in the literature [2], [9].

Postscript

At the time of manuscript submission, a flaw in the usage of the Coulomb gauge by Smythe [4] was uncovered by Michalski and Nevels [10]. The derivations of this paper were already in agreement with [10] on this point as presented by (4), and also on their corrections of Smythe [10, footnote 7], which are incorporated in (5).

References

[1] M. D. Deshpande, B. N. Das, and G. S. Sanyal, "Analysis of an end launcher for an *X*-band rectangular waveguide," *IEEE Trans. Microwave Theory Tech.*, vol. MTT-27, pp. 731–735, Aug. 1979.

[2] M. D. Deshpande and B. N. Das, "Analysis of an end launcher for a circular cylindrical waveguide," *IEEE Trans. Microwave Theory Tech.*, vol. MTT-26, pp. 672–675, Sept. 1978.

[3] R. F. Harrington, *Time Harmonic Electromagnetic Fields*. New York: McGraw-Hill, 1961, section 8.11.

[4] W. R. Smythe, *Static and Dynamic Electricity*, 3rd ed. New York: McGraw-Hill, 1968, section 13.03.

[5] L. Lewin, *Theory of Waveguides*. New York: Wiley, 1975, p. 139.

[6] R. M. Chisholm, "The characteristic impedance of trough and slab lines," *IRE Trans. Microwave Theory Tech.*, vol. MTT-4, pp. 166–172, July 1956.

[7] T. S. Saad, Ed., *Microwave Engineers' Handbook*, vol. 1. Dedham, MA: Artech, 1971.

[8] S. M. Saad, "Analysis and design of the colinear coaxial-to-rectangular waveguide transition," Andrew Corporation Tech. Rep. No. TMP-79-08, May 1979.

[9] T. Q. Ho and Y. Shih, "Analysis of microstrip line to waveguide end launchers," *IEEE Trans. Microwave Theory Tech.*, vol. 36, pp. 561–567, Mar. 1988.

[10] K. A. Michalski and R. D. Nevels, "On the use of the Coulomb gauge in solving source-excited boundary value problems of electromagnetics," *IEEE Trans. Microwave Theory Tech.*, vol. 36, pp. 1328–1333, Sept. 1988.

Saad Michael Saad (M'77–SM'82) was born in Alexandria, Egypt, on February 11, 1945. He received the B.Sc. and M.Sc. degrees from Alexandria University, Alexandria, Egypt, in 1965 and 1969, respectively, and the Ph.D. degree from the University of London, London, England, in 1974, all in electrical engineering.

He has held the positions of Research Assistant with University College, London, England (1970–1973), Researcher with the National Research Center, Cairo, Egypt (1974–1977), and Research Associate with the Remote Sensing Laboratory of the University of Kansas (1977–1978). Since 1978 he has been with the Andrew Corporation, Orland Park, IL, where he is now Section Leader-Waveguide Components.

Dr. Saad's professional career has centered on research and development in microwave passive components and antennas, with emphasis on numerical techniques and computer-aided design. In addition, he is interested in professional aspects of engineering, including issues of engineering ethics and the role of engineers in society. In pursuance of these interests he completed an M.A. in religious studies (focusing on ethics and society) at the University of Chicago in 1987. He is also concerned with engineering education and is currently an Adjunct Associate Professor at the University of Illinois at Chicago. Dr. Saad served as Chairman of the Chicago Chapter of the IEEE AP/MTT Societies (1983–1984). He is on the Steering Committee of the International IEEE-AP/URSI Symposium to be held in Chicago in 1992. He is a professional engineer registered in the state of Illinois, holds seven patents, and has authored "only" 15 technical publications.